Investigating the gluonic structure of nuclei via J/ψ scattering

A. Caldwell[1] and H. Kowalski[2,*]

[1]*Max Planck Institute for Physics, München, Germany*
[2]*Deutsches Elektronen-Synchrotron (DESY), D-22607 Hamburg, Germany*
(Received 23 September 2009; published 23 February 2010)

We propose to investigate the properties of nuclear matter by measuring the elastic scattering of J/ψ on nuclei with a high precision. J/ψ mesons are produced from photons emitted in high-energy electron-proton or electron-nucleus scattering in the low-x region. Their scattering on nucleons or nuclei is predominantly mediated by gluonic forces. The measurement could be performed at the future ENC, EIC, or LHeC facility.

I. INTRODUCTION

One of the main reasons why, after almost 80 years of investigations of nuclear structure, some of the basic properties are so poorly understood is the lack of proper tools to view inside nuclei. In the past, the most direct information about nuclear structure was obtained by scattering electron beams off nuclei. The electron is a very good probe because it penetrates into the nuclear interior without being absorbed. Unfortunately, electrons can only see the electric charge distributions. They are not sensitive to the distribution of strong fields that keep nuclei together. Another important source of information comes from the scattering of low-energy protons on nuclei. Protons sense the full matter distribution but they are themselves complicated objects whose interactions with matter are not very well known. Our understanding of strong interactions is currently only robust at distances much smaller than the proton size, where perturbative QCD is applicable. Although lattice gauge theory has firmly established that QCD is the correct theory of strong interactions at large distances, its applications to hadronic interactions are only now being developed [1–3].

In recent years the Hadron-Electron Ring Accelerator (HERA) has shown that, in deep inelastic electron-proton scattering at low x, up to 20% of events are of diffractive origin.[1] This is comparable to the rate of elastic reactions in hadron-hadron scattering at high energy. In hadronic reactions the rate of elastic and inelastic events is connected by the optical theorem. Before HERA, the optical theorem was not expected to play any role in electron-proton scattering because the elastic ep component is miniscule. The abundance of diffractive (i.e., quasielastic) processes seen at HERA therefore indicates that some intermediate states have to be formed to which the optical theorem can be applied. The theoretical framework that naturally describes the formation of such intermediate states is the dipole picture. Dipoles are small quark-antiquark pairs that interact by color exchange. In contrast to hadron scattering, where the projectiles are complicated, color dipoles are simple objects. Their creation,

interaction, and annihilation have a simple description in perturbative QCD combined with QED. A multitude of HERA measurements such as inclusive cross sections, charm production, diffraction, jet production, vector-meson production, and DVCS cross sections are accurately explained within the dipole picture [4–13].

A particular final state into which a dipole transforms acts as an analyzer. For example, jets select very small dipoles, J/ψ production selects charm-anticharm dipoles, ρ mesons $u\bar{u}$ or $d\bar{d}$ dipoles, and so on. For nuclear structure investigations the most interesting process is the scattering of small dipoles. The smallness of the dipole assures that the interaction with the nucleon is well described by perturbative QCD. In the low-x region small dipoles interact with the nucleon by gluon exchange only. The color exchange is of short range, in contrast to the interaction of electromagnetic dipoles. Of particular interest is the elastic scattering of color dipoles because the transverse deflection of the dipole measures the spatial distribution of the gluonic matter.

In this paper we concentrate on the measurement of exclusive J/ψ vector-meson photoproduction. The J/ψ meson is a bound state of a charm quark-antiquark pair and therefore the corresponding dipole is naturally small. The cross section is relatively high because we take photoproduction.

In nuclei, the small charmed dipole presumably scatters on individual nucleons. Despite the high energies involved, the nucleus will frequently remain intact because the large absorption cross section together with the optical theorem assures that the scattering process has to be coherent in about 15% of cases [13,21]. Because the charmed quark dipole interacts almost completely via two-gluon exchange with matter, the deflection of the J/ψ measures directly the **intensity** and the **spatial distribution** of the strong field that keeps the nucleus together. This will allow us to see precisely the structure of gluonic fields, which has never been seen before.

This paper is organized as follows. In Sec. II we give an overview of the main properties of the dipole interaction and summarize in some detail the existing experimental results. In Sec. III we discuss the properties of J/ψ as a probe of proton and nuclei. In Sec. IV we discuss the J/ψ production cross section within potential detector acceptances, and in Sec. V we discuss the detector requirements necessary to perform a precise p_T measurement and the experimental requirements

---

*henri.kowalski@desy.de
[1]Here diffraction means that the proton stays intact.

necessary to assure the elastic signature. In Sec. VI we summarize the results and in Sec. VII we conclude. In the Appendix we give a derivation of the dipole representation in a simple case of elastic photon-proton scattering.

II. DIPOLE DESCRIPTION OF DEEP INELASTIC SCATTERING (DIS) REACTIONS

Dipole interactions are, in a way, as fundamental as Rutherford scattering. In Rutherford scattering the incoming electron emits a virtual photon that scans the charge distribution of the nuclear target. In elastic dipole scattering the incoming electron emits a virtual photon that turns into a small quark-antiquark pair. In leading-order QCD, at large virtuality scales and high energies, the $q\bar{q}$ pair interacts elastically with the nucleon by exchanging *two* gluons with large transverse momenta, $\vec{l}$ and $\vec{l} + \vec{\Delta}$. The transverse momenta of the gluons cannot be directly observed, however, their difference $\vec{\Delta}$ is measurable in elastic vector-meson scattering because it is equal to the difference between the transverse momentum of the incoming virtual photon and the final vector meson. The two-gluon interaction leads in QCD (together with QED) to the dipole representation. In the Appendix we derive the dipole representation from Feynman diagrams in a simple case of virtual photon-proton elastic scattering, when $\vec{\Delta} = 0$. In the following we discuss the main properties of the dipole representation.

A. Dipole representation

The dipole interaction proceeds in three stages: first, the incoming virtual photon fluctuates into a quark-antiquark pair; next, the $q\bar{q}$ pair elastically scatters on the target; and, finally, the $q\bar{q}$ pair recombines to form a final state. The creation, scattering, and recombination of the dipole occur in different space-time regions because the lifetime τ of the $q\bar{q}$ fluctuation is very long. In the proton rest frame, $\tau \approx 1/m_p x$. Even at $x = 10^{-2}$ this corresponds to a distance of $\sim$20 fm, which is larger than the size of all nuclei, $R \approx 1.2 \cdot A^{1/3}$ fm. In addition, owing to high energies, the transverse positions of the quark and antiquark do not change in the scattering process so that the dipole does not change its size (see Appendix).

The amplitude of the elastic photon-proton scattering, $\gamma^* p \to \gamma^* p$, $\mathcal{A}^{\gamma^* p}(x, Q, \Delta)$, is therefore the product of amplitudes of these three subprocesses integrated over the dipole variables $\vec{r}$ and z:

$$
\begin{aligned}
&\mathcal{A}^{\gamma^* p}(x, Q, \Delta) \\
&= \sum_f \int d^2\vec{r} \int_0^1 \frac{dz}{4\pi} \Psi^*(r, z, Q) \mathcal{A}_{q\bar{q}}(x, r, \Delta) \Psi(r, z, Q),
\end{aligned}
\tag{1}
$$

where $\Psi(r, z, Q)$ denotes the amplitude for the incoming virtual photon, with virtuality Q, to fluctuate into a quark-antiquark dipole with flavor f.[2] The wave function is deter-

_____

[2]We suppress references to photon helicities here for simplicity.

mined from light cone perturbation theory to leading order in the fermionic charge; see the Appendix. The amplitude for the $q\bar{q}$ to recombine to a virtual photon is $\Psi^*(r, z, Q)$. $\mathcal{A}_{q\bar{q}}(x, r, \Delta)$ is the elementary amplitude for the scattering of a dipole of size r on the proton, $\vec{\Delta}$ denotes the transverse momentum transferred from the dipole to the target, and x is the Bjorken variable. The sum should be taken over all quark flavors f, including charm. For a charmed quark the definition of the Bjorken $x = x_B$ should be replaced by $x = x_B[1 + (4m_{ch}^2/Q^2)]$ to take into account charm threshold effects. For similar reasons, in the case of vector-meson production, $x = x_B[1 + (M_V^2/Q^2)]$.

The elementary elastic amplitude $\mathcal{A}_{q\bar{q}}$ is defined such that the elastic differential cross section for $q\bar{q}$-pair scattering on the proton is

$$
\frac{d\sigma_{q\bar{q}}}{dt} = \frac{1}{16\pi} |\mathcal{A}_{q\bar{q}}(x, r, \Delta)|^2,
\tag{2}
$$

where $t = -\vec{\Delta}^2$. The notation follows the conventions of Refs. [9] and [18]. Elastic dipole scattering is connected by the optical theorem to the total cross section for photon-proton or photon-nucleus scattering. To evaluate the connections between the total cross section and various diffractive reactions, it is convenient to work in coordinate space and define the S-matrix element at a particular impact parameter b:

$$
\begin{aligned}
\mathcal{A}_{q\bar{q}}(x, r, \Delta) &= \int d^2\vec{b} \, e^{-i\vec{b}\cdot\vec{\Delta}} \mathcal{A}_{q\bar{q}}(x, r, b) \\
&= i \int d^2\vec{b} \, e^{-i\vec{b}\cdot\vec{\Delta}} 2[1 - S(x, r, b)].
\end{aligned}
\tag{3}
$$

This corresponds to the intuitive notion of impact parameter when the dipole size is small compared to the size of the proton. The optical theorem then connects the total cross section for $q\bar{q}$-pair scattering on the proton to the imaginary part of the forward scattering amplitude:

$$
\begin{aligned}
\sigma_{q\bar{q}}(x, r) &= \text{Im}\, \mathcal{A}_{q\bar{q}}(x, r, \Delta = 0) \\
&= \int d^2\vec{b} \, 2[1 - \text{Re}\, S(x, r, b)].
\end{aligned}
\tag{4}
$$

The integration over $\vec{b}$ of the S-matrix element motivates the definition of the differential dipole cross section as

$$
\frac{d\sigma_{q\bar{q}}}{d^2\vec{b}} = 2[1 - \text{Re}\, S(x, r, b)].
\tag{5}
$$

The total cross section for $\gamma^* p$ scattering, or equivalently F_2, is obtained, using Eqs. (1) and (4), by integrating the dipole cross section with the photon wave functions:

$$
\begin{aligned}
\sigma_{T,L}^{\gamma^* p}(x, Q) &= \text{Im}\, \mathcal{A}_{T,L}^{\gamma^* p}(x, Q, \Delta = 0) \\
&= \sum_f \int d^2\vec{r} \int_0^1 \frac{dz}{4\pi} (\Psi^*\Psi)_{T,L}^f \sigma_{q\bar{q}}(x, r),
\end{aligned}
\tag{6}
$$

where the subscript T or L denotes the transverse or longitudinal polarization of the incoming photon, respectively. For completeness we also give the relation between the F_2 structure function and the $\gamma^* p$ cross section at low x:

$$
F_2(x, Q^2) = \frac{Q^2}{4\pi^2 \alpha_{em}} (\sigma_T + \sigma_L).
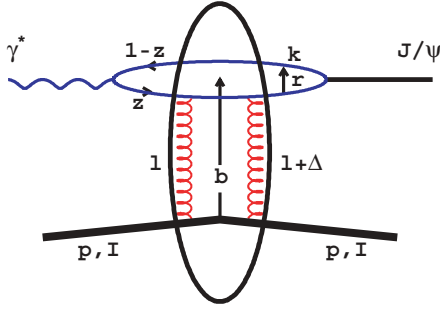$$

FIG. 1. (Color online) Elastic scattering of a J/ψ meson on a proton or ion in the dipole representation.

Elastic vector-meson production appears in a similarly transparent way. The amplitude is given by

$$A_{\gamma^* p \to pV}(\Delta)$$
$$= \int d^2r \int \frac{dz}{4\pi} \int d^2b \, \Psi_V^* \Psi \exp(-i\vec{b} \cdot \vec{\Delta}) 2[1 - S(b)]. \tag{7}$$

Assuming that the S-matrix element is predominantly real, we may substitute $2[1 - S(b)]$ with $d\sigma_{q\bar{q}}/d^2b$. Then the elastic cross section is

$$\frac{d\sigma^{\gamma^* p \to Vp}}{dt}$$
$$= \frac{1}{16\pi} \left| \int d^2r \int \frac{dz}{4\pi} \int d^2b \, \Psi_V^* \Psi \exp(-i\vec{b} \cdot \vec{\Delta}) \frac{d\sigma_{q\bar{q}}}{d^2b} \right|^2. \tag{8}$$

Equations (6) and (8) determine the total DIS cross sections and the exclusive diffractive vector-meson production cross section. Figure 1 is a diagram of the dipole scattering when the final state is a J/ψ meson.

B. Dipole cross sections

The universal dipole cross section $d\sigma_{q\bar{q}}/d^2\vec{b}$ contains all the information about the gluon content of the target and the QCD evolution of the gluon density. Its particular form depends on the evolution schema. In the DGLAP formalism, the dipole cross section for small dipoles is given by[3]

$$\frac{d\sigma_{q\bar{q}}}{d^2b} = \frac{\pi^2}{3} r^2 \alpha_s(\mu^2) \, xg(x, \mu^2) \, T(b). \tag{9}$$

Here $xg(x, \mu^2)$ is the gluon density and μ^2 denotes the evolution scale. The starting scale is denoted μ_0^2. The scale is given by the inverse of the dipole size and is usually taken as $\mu^2 = (4/r^2) + \mu_0^2$, to stabilize the α_s behavior for large dipoles. The function $T(b)$ is the transverse profile of the gluon density of the proton. It is convenient to write the gluon density in a semifactorized form, $xg(x, \mu^2)T(b, x)$. Because the x dependence of $T(b)$ is weak, it is omitted in the following

---

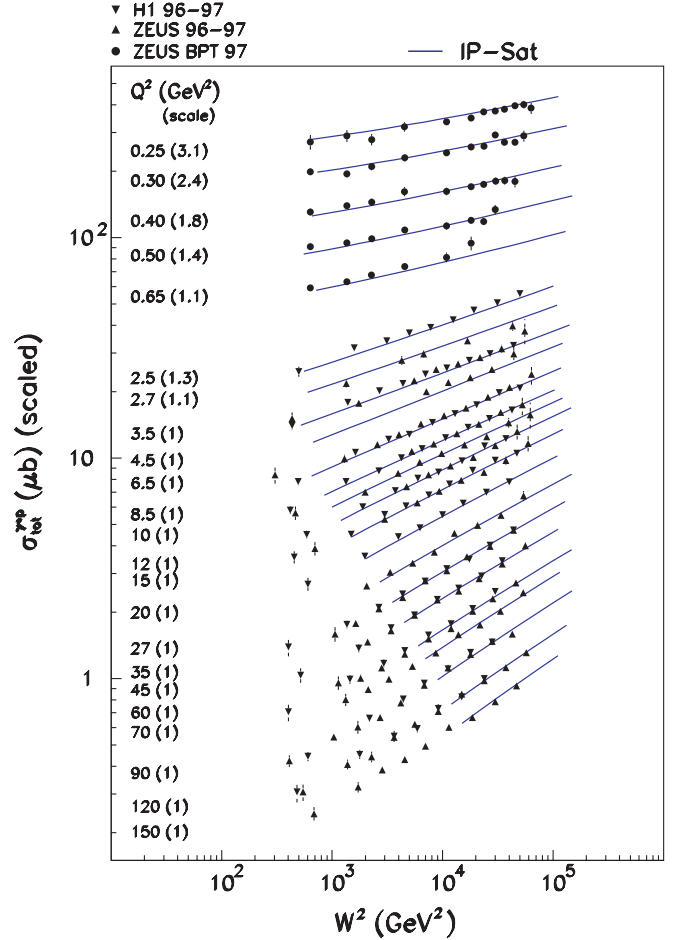[3]The derivation of the dipole cross section is given in the Appendix.

FIG. 2. (Color online) The $\gamma^* p$ cross section as a function of W^2. Solid lines show the dipole fit to the data [17] in the low-x region, $x < 10^{-2}$.

discussion. At every x the transverse profile is normalized to 1, $\int d^2b T(b) = 1$. The parameters of the gluon density are determined from the fit to the total inclusive DIS cross section measured at HERA using Eq. (6). The fit is shown in Fig. 2. The gluon density at a scale μ_0^2 is parametrized by $xg(x, \mu_0^2) = c \cdot x^{-\lambda}$. The three free parameters are c, λ, and μ_0^2. The predictions of the model, at low Q^2 values, also depend on the assumption on the quark masses, m_f. Other schemas, like the CGC evolution and Regge parametrizations, also lead to a successful description of the data [19,20,31]. More details are given in Refs. [18] and [19].

The transverse profile is assumed to have a two-dimensional Gaussian form:

$$T(b) = \frac{1}{2\pi B_G} \exp(-b^2/2B_G), \tag{10}$$

as the measured t distributions were found to be well described by the exponentially falling distribution, $d\sigma_{VM}^{\gamma^* p}/dt \propto \exp(-B_D|t|)$; see Fig. 3.[4] The coefficient B_D is not exactly

---

[4]The Fourier transform of a Gaussian in $\vec{b}$ is a Gaussian in $\vec{\Delta}$ corresponding to an exponential in t.
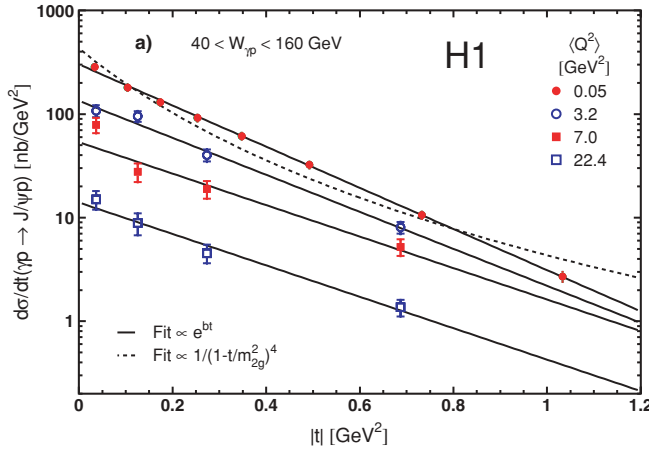
FIG. 3. (Color online) Differential cross section for elastic J/ψ production [25].

equal to B_G because the size of the vector meson is not negligible (see the discussion in Sec. II D). In addition, the observed coefficient B_D shows some x dependence (e.g., in J/ψ photoproduction) and so B_G should be x dependent (see the discussion in Sec. III A). We note also that the fit with the dipole form factor, $d\sigma/dt \propto 1/(1 - t/M^2)^4$, which is usually used to parametrize the proton form factors does not describe the data appropriately [25].

The dipole cross section, Eq. (9), is propotional to the dipole area r^2 and the gluon density seen by the dipole, $xg(x, \mu^2)$. It is therefore a measure of the gluon density. When either the dipole size or the gluon density is not small, it is convenient to use the eikonalized form of the dipole cross section to take into account possible saturation effects:

$$\frac{d\sigma_{qq}}{d^2b} = 2\left(1 - \exp\left(-\frac{\pi^2 r^2 \alpha_s(\mu^2)\, xg(x, \mu^2)\, T(b)}{2 \cdot 3}\right)\right)$$
$$= 2\left(1 - \exp\left(-\frac{\Omega}{2}\right)\right). \quad (11)$$

Here Ω denotes the opacity, which is equal to the right side of Eq. (9). This formula is called the Glauber-Mueller dipole cross section. A diffractive cross section of this type was used by Glauber [26] about 50 years ago to study the diffractive dissociation of deuterons and reintroduced by Mueller [27] to describe dipole scattering in deep inelastic processes. In contrast to Glauber scattering, in DIS the functional form of the opacity is known from QCD.

C. Deeply virtual Compton scattering (DVCS) and vector-meson production

The elastic cross section, Eq. (8), was derived under the assumption that the dipole size is much smaller than the proton size. For dipoles of a size r the explicit QCD calculation [45] shows that $\vec{\Delta}$ conjugates to $\vec{b} + (-z)\vec{r}$. Therefore, the cross section is sensitive not only to the proton impact factor b, but also to the dipole size r. Thus, the modified dipole cross

section is

$$\frac{d\sigma^{\gamma^* p \to Vp}}{dt} = \frac{1}{16\pi}\left| \int d^2r \int \frac{dz}{4\pi} \int d^2b\, \Psi_V^* \Psi \exp(-i[\vec{b} \right.$$
$$\left. + (1-z)\vec{r}]\cdot\vec{\Delta})\frac{d\sigma_{q\bar{q}}}{d^2b}\right|^2. \quad (12)$$

This cross section can also be used to describe the DVCS process, for which the final state consists of the scattered electron, the proton, and a real photon. The wave function for the outgoing state is just the amplitude $\Psi^*(Q^2 = 0)$ for the real photon. Equation (12) gives, after a small correction for the real part[5] and skewedness[6] are applied, an absolute prediction for the DVCS process. The prediction is shown along with HERA data in Fig. 4. The figure shows an impressive agreement between the dipole model predictions and the data if we realize that two very different processes are described with the same amplitudes; the average event that contributes to the total cross section has about 40 particles in the final state, while the DVCS event has just a proton, a photon, and an electron. The wave function of the final state, $\Psi^*(Q^2 = 0)$, is very different from that of the incoming virtual photon. And yet all the distributions and the absolute event rates of the DVCS process are properly described. This means that the net effects of possible higher-order QCD radiative corrections [28] or possible kinematical corrections [30] have to be small or are consistently absorbed into the gluon density.

Successful comparisons of the inclusive diffractive cross sections with the dipole model predictions have been performed in several investigations [7,8,13,31]. Inclusive diffraction denotes the sum of all processes in which the proton remains intact. Because the summation is over a complete set of states, the cross section depends only on the photon wave functions. However, the dipole cross section in this case has to take into account also the possible $q\bar{q}g$ Fock state, which makes the comparison less clean than in the DVCS case. Nevertheless, comparison of the cross sections with the predictions again works very well [13]. The same is also true for the comparison with the diffractive jet cross sections [37].

Further support for the validity of the dipole picture comes from the very good agreement of the predicted vector-meson cross sections with the data, shown in Fig. 5. The vector- meson wave functions are constructed according to a standard procedure developed in Refs. [43] and [44]. They are educated guesses based on general considerations described in Refs. [11] and [18]. The only phenomenological input that is necessary is obtained from the measured electronic decay width of the vector meson. The very good agreement

---

[5]The derivation of the cross section for exclusive vector-meson production or DVCS relies on the assumption that the scattering amplitude is purely imaginary. The real part of the amplitude can be accounted for by multiplying the exclusive cross section by a small correction factor given in Ref. [11].

[6]For vector-meson production or DVCS, one should use the off-diagonal gluon densities, as here the two gluons carry different fractions x and x' of the proton momentum. This effect can be taken into account by multiplying the gluon distribution $xg(x, \mu^2)$ by a correction factor R_g given in Ref. [29].
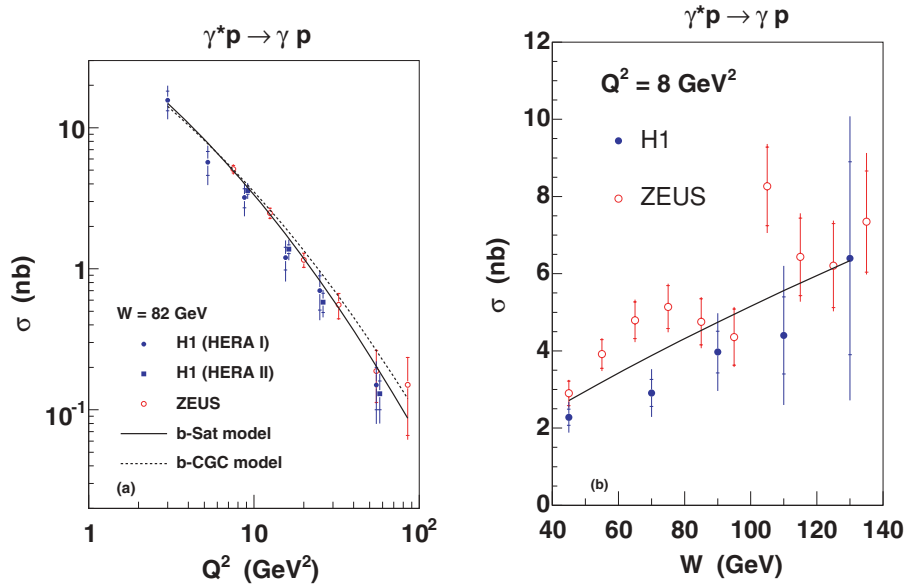
FIG. 4. (Color online) Total DVCS cross sections σ as a function of Q^2 (a) and W (b) [32] compared to predictions from the b-Sat and b-CGC models [19].

between data and dipole model predictions means that the vector-meson wave functions were properly estimated. This is further supported by the excellent description of the σ_L/σ_T ratio as a function of Q^2 for the J/ψ and ϕ vector mesons [18]. In the case of ρ mesons this ratio is not so well described. This can be attributed to the complicated dynamic of ρ decay into pions.

D. The t distributions

At HERA, the distributions of the square of the momentum transfer, $t = -\vec{\Delta}^2$, have been measured in exclusive vector-meson and DVCS processes. The value of t is usually determined from the p_T imbalance of the final-state particles seen in the detector. The t distributions have also been measured using forward proton spectrometers for all diffractive processes. Forward spectrometers, however, have a relatively low acceptance.

All measured t distributions are very well described by the exponential dependence $d\sigma/dt \propto \exp(-B_D|t|)$. The t range used in the fit to the vector-meson differential cross sections is typically limited to $|t| < 1$ GeV^2 to avoid regions where large corrections were applied to account for the proton dissociation process. B_D is related to the size of the interaction region, as discussed here. It is sensitive to the gluonic proton shape and to the sizes of the dipoles contributing to the process. The dipole sizes depend, through the incoming and outgoing wave functions, on the Q^2 value and the vector-meson spatial extension.

Figure 6 shows B_D as a function of W for J/ψ photo-production. The average value of B_D from this process was used to fix the B_G parameter of the proton shape in the b-Sat model to $B_G = 4.0$ GeV^{-2}. The model then allows prediction of the expected B_D values for other processes, like DVCS and ϕ and ρ production. The predictions are compared to data in Fig. 7. The value of B_D depends considerably on Q^2 and the
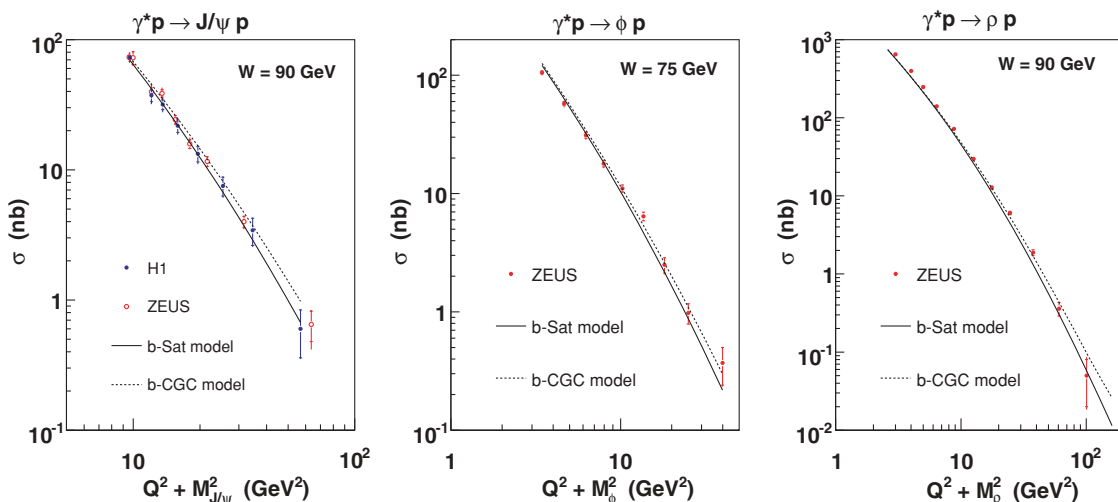

FIG. 5. (Color online) Total cross section σ vs. $(Q^2 + M_V^2)$ for exclusive J/ψ [25,33], ϕ [35], and ρ [36] meson production compared to predictions from the b-Sat and b-CGC models using the "boosted Gaussian" vector-meson wave function [19].
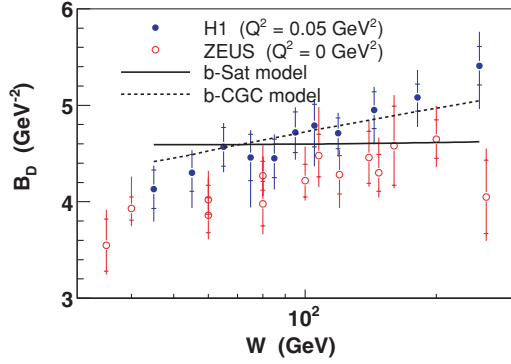
FIG. 6. (Color online) The t slope parameter B_D vs. W for J/ψ photoproduction.

type of process, as the effective sizes of vector mesons and of the DVCS photon differ substantially. The dipole model reproduces the changes in the value of B_D very well.

As shown in Fig. 6 the value of B_D in J/ψ photoproduction shows some W dependence. This can be attributed to QCD evolution effects. In the DGLAP evolution scheme, owing to strong ordering, the increase in B_D with decreasing $x \approx M_{J/\psi}^2/W^2$ is expected to be negligible [38], as in the b-Sat model. In the BFKL evolution scheme the evolution in x could lead to a small increase in the size of the interaction area. This was taken into account in the b-CGC model, which is based on a phenomenological approach to the BFKL and BK equations [18–20]. Alternatively, the variation of B_D with W can also be attributed to the increase in the contribution of the "pion cloud" at low x [39].

III. J/ψ AS A PROBE OF PROTON AND NUCLEI

The properties of diffractive processes described in the previous section single out J/ψ photoproduction as an ideal probe for investigation of nuclear properties, for three

main reasons.

(i) The J/ψ meson provides the smallest probe compared to the other diffractive processes measured at HERA. This can be seen directly from measurement of the sizes of the interaction region B_D shown in Figs. 6 and 7.

(ii) The observed number of well-measured events is substantially larger for J/ψ photoproduction than for other exclusive diffractive processes with a similar probe size.[7] In the central region of the H1 and ZEUS detectors, the number of well-measured $\gamma p \to J/\psi\, p \to \mu\mu\, p$ and $\gamma p \to J/\psi\, p \to ee\, p$ events is about 10 times higher than for $\gamma^* p \to \rho p \to \pi\pi\, p$ and a factor of 40 higher than for $\gamma^* p \to \phi p \to KK\, p$ processes with $Q^2 + M_V^2 > 10$ GeV^2. For the DVCS reaction, with $Q^2 > 10$ GeV^2, this factor is about 100.

(iii) The J/ψ meson decays with a probability of 12% into a leptonic pair, $\mu^+\mu^-$ or e^+e^-. These are very clean final states that emerge from quark annihilation. It can be measured well in the detector because the J/ψ is a very narrow resonance. The ρ meson decays mostly into a pair of pions, which can also be measured well. However, this is a strong decay, the ρ width is large, and the decay mechanism is more complicated than in the J/ψ case. This may make this process less suitable as a probe of nuclear properties.

---

[7]This is because the cross section for the electroproducion process is approximately proportional to $\log(Q_{max}^2/Q_{min}^2)$ and to the photoproduction cross section $\sigma^{\gamma p}$. In the ZEUS and H1 measurements of J/ψ photoproduction, $Q_{min}^2 \approx 10^{-12}$ GeV^2 and $Q_{max}^2 \approx 1$ GeV^2. In this Q^2 region the photoproduction cross section $\sigma^{\gamma p}$ is almost constant. For the ρ, ϕ, or DVCS process one has to require that $Q_{min}^2 \approx 10$ GeV^2 to ensure that the interaction is mediated by the small dipoles. In addition, the virtual photon-proton cross section decreases quickly with increasing Q^2, $\sigma^{\gamma^* p} \sim 1/(M_V^2 + Q^2)^n$, with $n \approx 3$, which effectively limits the Q^2 range.
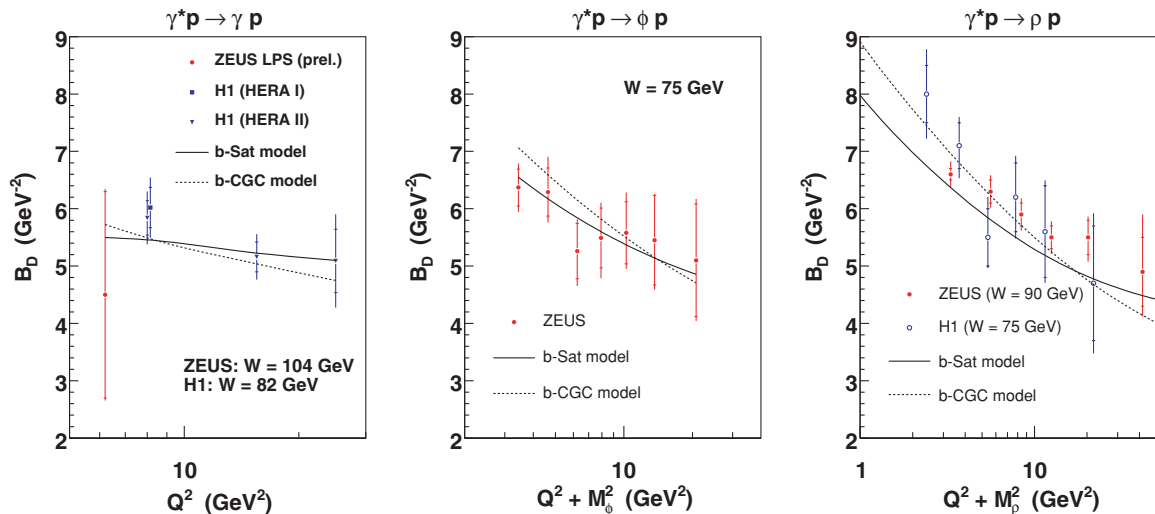

FIG. 7. (Color online) The t slope parameter B_D for the DVCS process and for exclusive ϕ [35] and ρ [34,36] meson production compared to predictions from the b-Sat and b-CGC models.

A. Proton radius

To show the potential of J/ψ photoproduction as a probe of the properties of matter we discuss here a classic nuclear physics subject, determination of the proton radius. The smallest sizes of the interaction region, B_D, are measured at HERA in the exclusive J/ψ photoproduction process, in agreement with the dipole model expectations. The t distribution of this process is also one of the most precisely measured at HERA. In the following we determine the proton radius using data on this process.

The observed values of B_D in the H1 and ZEUS experiments show an increase with growing energy W. This increase is parametrized in the HERA experiments as

$$B_D(W) = b_0 + 4\alpha' \cdot \log(W/90 \text{ GeV}). \qquad (13)$$

For ZEUS,

$$b_0 = 4.15 \pm 0.05^{+0.30}_{-0.18} \text{ GeV}^{-2},$$
$$\alpha' = 0.115 \pm 0.018^{+0.008}_{-0.015} \text{ GeV}^{-2},$$

and for H1,

$$b_0 = 4.63 \pm 0.06^{+0.043}_{-0.163} \text{ GeV}^{-2},$$
$$\alpha' = 0.164 \pm 0.028^{+0.030}_{-0.030} \text{ GeV}^{-2}.$$

The W region extends from 30 to 170 GeV and the values of B_D increase with W by about 25%, owing to QCD evolution effects. The proton radius should be related to the value of B_D without this effect, that is, to the value of B_D at W near the threshold. However, it is not known whether Eqs. (13) can be extrapolated to below $W = 30$ GeV. Therefore we evaluate the proton radius from the lowest observed value of B_D at $W = 30$ GeV. This value of W also corresponds to the x value, $x = 10^{-2}$, up to which the dipole picture was successfully tested.

At $W = 30$ GeV the size of the interaction region is $B_D = 3.64 \text{ GeV}^{-2}$ for ZEUS and $B_D = 3.91 \text{ GeV}^{-2}$ for H1. We can combine these values into

$$B_D(W = 30 \text{ GeV}) = 3.78 \pm 0.3 \text{ GeV}^{-2}.$$

As error we take the difference between the ZEUS and the H1 values.

The proton size is related to the value of B_G, which is smaller than B_D, owing to the contribution of the size of the J/ψ. The difference at $W = 30$ GeV is $B_D - B_G = \Delta B = 0.6 \text{ GeV}^{-2}$ [18] and is almost independent of W. The theoretical error can be estimated by evaluating B_G with two different wave functions as $\Delta B = \pm 0.2 \text{ GeV}^{-2}$ [18].

The corresponding proton Gaussian width is $B_G = 3.18 \pm 0.4 \text{ GeV}^{-2}$, where we added the theoretical and experimental errors in quadrature. The transverse proton radius is then

$$\sqrt{\langle b^2 \rangle} = \sqrt{\int d^2\vec{b}\, b^2 T_G(b)} = \sqrt{2 \cdot B_G} = 0.50 \pm 0.03 \text{ fm}.$$

The proton radius is usually determined from the electromagnetic charge form factor,

$$G_E(t) = 1 + \tfrac{1}{6}\langle r_p^2 \rangle t + O(t^2),$$

and

$$\langle r_p^2 \rangle = 6 \cdot \left.\frac{dG_E(t)}{dt}\right|_{t=0}.$$

This is the three-dimensional proton radius; the transverse proton radius is given by

$$\langle b_p^2 \rangle = 4 \cdot \left.\frac{dG_E(t)}{dt}\right|_{t=0}.$$

Therefore the transverse proton radius is related to the three-dimensional proton radius by $\langle b_p^2 \rangle = 2\langle r_p^2 \rangle/3$ [39,40]. Guided by this we obtain the three-dimensional proton radius as measured by the exclusive J/ψ photoproduction,

$$\sqrt{\langle r_{2g}^2 \rangle} = \sqrt{3 \cdot B_G} = 0.61 \pm 0.04 \text{ fm}.$$

We call this radius r_{2g} to indicate that it is determined in the two-gluon exchange process.

The two-gluon proton radius, r_{2g}, is much smaller than the charged proton radius determined from the electromagnetic form factor G_E, $r_p = 0.875 \pm 0.007$ fm. One could argue that it is more appropriate to compare the two-gluon proton radius to the proton radius that is determined from the Dirac form factor F_1, $r_F = 0.81$ fm, instead of G_E, as proposed in Ref. [40]. This value is smaller than the standard charged proton radius because the Dirac form factor describes only the spin nonflip interactions (in the infinite momentum frame). Nevertheless, the spin-preserving proton radius is still substantially larger than the two-gluon proton radius.

It is expected that the value of the proton radius is process dependent because the current that tests the proton itself has a structure that depends on its quantum numbers [41]. The smallest proton radius is determined from the axial form factor G_A measured in neutrino scattering, $\nu p \rightarrow \mu p$. This is called the axial radius and has the value $r_A = 0.675 \pm 0.02$ fm [41]. The smallness of this radius can be attributed to the fact that the axial current is not coupling to the pion cloud surrounding the bulk of the proton [39]. It is interesting to observe that the two-gluon radius is still smaller than the axial radius despite the fact that the two-gluon intermediate state couples as well to the bulk of the proton as to the surrounding pions.

B. The gluonic structure of nuclei

Measurements of diffractive processes could become an important source of information on the gluonic structure of nuclei and high-density QCD. The interaction of a dipole with a nucleus can be viewed as a sum of dipole scatterings of the nucleons forming the nucleus. The size of the charmed dipole in elastic J/ψ scattering is about 0.15 fm [17], that is, it is much smaller than the nucleon radius. It is therefore possible that dipoles interact with objects smaller than nucleons, for example, with constituent quarks or hot spots. Nevertheless, for the sake of illustration, we take here the conventional point of view and assume that the nucleus is built out of nucleons and that dipoles scatter on the ensemble of nucleons. We discuss the dipole-nucleus scattering using two examples to show the potential of possible nuclear investigations. To simplify the discussion multiple scattering effects are ignored, justified by the small size of the J/ψ dipole; see also Sec. III C.
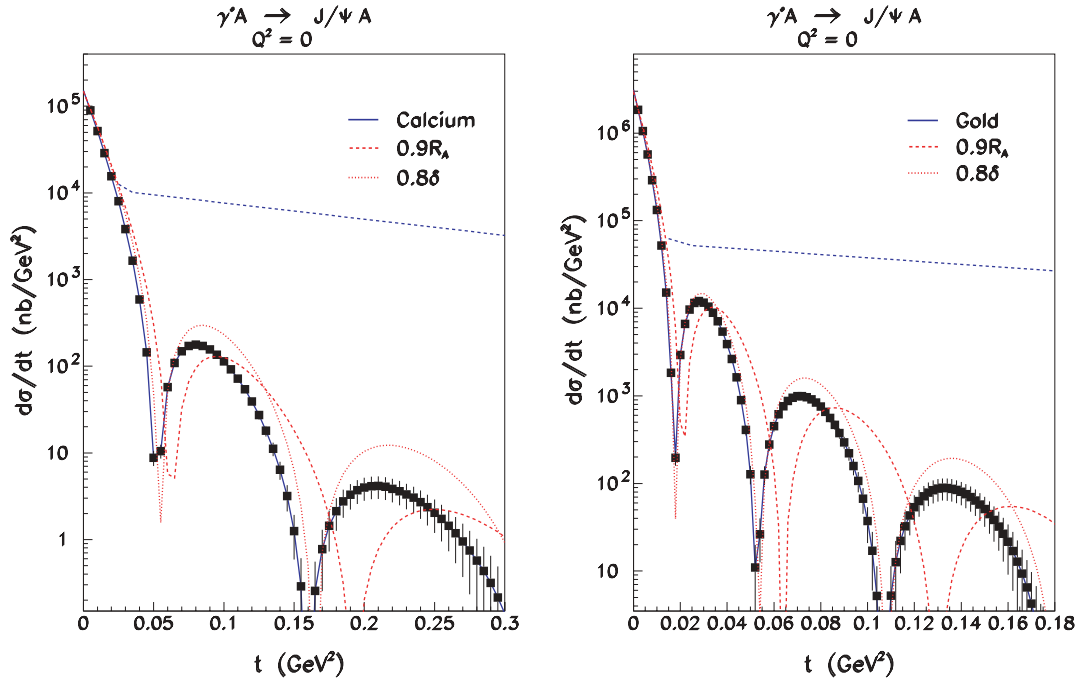
FIG. 8. (Color online) Prediction of the dipole model for the t distribution of coherent J/ψ photoproduction on nuclei assuming that the single-nucleon distribution can be identified with the Woods-Saxon distribution given in the Appendix. Statistical errors of the simulated measurements are based on the assumed collected sample of 10^6 events. The dashed line near the top shows the sum of the coherent and incoherent process in the case of no correlations.

In the first example we consider elastic scattering on the nucleus [17,21]. This is a coherent scattering process, as the nucleus remains in its ground state. Ignoring possible multiple scattering effects, the dipole scattering amplitude for a given configuration of nucleons $\{\vec{b}_i\}$, using Eqs. (9) and (10), is given by

$$\frac{d\sigma_{q\bar{q}}^A}{d^2b} = \sigma_p \sum_{i=1}^{A} \frac{e^{-(\vec{b}-\vec{b}_i)^2/2B_p}}{2\pi B_p}, \qquad (14)$$

where A denotes the number of nucleons in the nucleus, B_p is the diffractive slope of the proton, and σ_p is the total proton dipole cross section. The Fourier transform of this amplitude is

$$\int d^2b\, e^{-i\vec{b}\cdot\vec{\Delta}} \frac{d\sigma_{q\bar{q}}^A}{d^2b} = \sigma_p \sum_{i=1}^{A} e^{-i\vec{b}_i\cdot\vec{\Delta}} \cdot e^{-B_p\cdot\Delta^2/2}. \qquad (15)$$

Here we changed the integration variable from $\vec{b}$ to $\vec{b}-\vec{b}_i$ while integrating each term of the sum. We obtain the matrix element for elastic scattering $(q\bar{q})+A_0 \rightarrow (q\bar{q})+A_0$ by averaging over all configurations of the nucleus ground state:[8]

$$-iA_{A_0\rightarrow A_0}^{q\bar{q}} = \sigma_p e^{-B_p\cdot\Delta^2/2} \sum_{i=1}^{A} \int d^2\vec{b}_1 \cdots d^2\vec{b}_A$$
$$\times \Psi_{A_0}^*(\vec{b}_1\cdots\vec{b}_A)\Psi_{A_0}(\vec{b}_1\cdots\vec{b}_A) \cdot e^{-i\vec{b}_i\cdot\vec{\Delta}}. \qquad (16)$$

---

[8]To simplify the notation we write $\Psi(\ldots)$ as a function of the transverse variables, $\vec{b}_i$, only; that is, we assume that the longitudinal dimensions, z_i, are already integrated out.

We define the single-nucleon distribution as

$$\int d^2\vec{b}_2 \cdots d^2\vec{b}_A d^2\Psi_{A_0}^*(\vec{b}_1\cdots\vec{b}_A)\Psi_{A_0}(\vec{b}_1\cdots\vec{b}_A) = T_A(b_1), \qquad (17)$$

with normalization $\int d^2b_1 T_A(b_1) = 1$. Because the wave function for protons and neutrons is completely antisymmetric and the difference between proton and neutron is presumably small, we assume that $T_A(b_1) = T_A(b_i)$. The cross section for the coherent dipole scattering is then given by

$$\frac{d\sigma_{A_0\rightarrow A_0}^{q\bar{q}}}{dt} = \frac{A^2\sigma_p^2}{16\pi} e^{-B_p\cdot\Delta^2} \cdot \left|\int d^2b\, T_A(b)e^{-i\vec{b}\cdot\vec{\Delta}}\right|^2, \qquad (18)$$

that is, it is proportional to the square of the Fourier transform of the single-nucleon distribution.

The cross sections for coherent J/ψ scattering on nuclei—computed in the dipole model by averaging the dipole cross section, Eq. (18), over the incoming photon and outgoing J/ψ wave functions—are shown in Fig. 8 as a function of t. Note that in the nuclear case, the size of the vector meson can be ignored. We assumed here that the single-nucleon distribution can be identified with the Woods-Saxon distribution; see the Appendix. The diffractive slope at $t=0$ depends on the size of the system. Figure 8 shows, for small $t \sim 1/R_A^2$, a very steep t dependence, $\sim\exp(-tR_A^2/3)$, and then several diffractive minima. For larger nuclei the Woods-Saxon shapes are approximately similar to a box of size R_A. The Fourier transform of a box is given by the Bessel function $J_1(R_A \cdot \Delta)$,

which has zeros at $R_A \cdot \Delta = 3.8, 7.0, 10.2, \ldots$.[9] This gives the approximate positions of the diffractive minima for the exclusive J/ψ photoproduction on calcium ($A = 40$) and gold ($A = 197$) shown in Fig. 8. The parameters of the Woods-Saxon distribution, nuclear radius and skin depth, were determined mainly by scattering of the charged matter and can be fairly different when measured in dipole interactions. We therefore plot in Fig. 8 the predictions computed with slightly altered values of these parameters.

In the second example we evaluate incoherent dipole scattering [13,21,22,46]. We start with the quasielastic scattering of a dipole on a nucleus,

$$(q\bar{q}) A_0 \to \sum_n (q\bar{q}) A_n,$$

where A_n can be either a ground state, or any excited nuclear state, or any breakup of the nucleus into nucleons or nucleonic fragments. Pion and other hadronic production is not allowed. As in the elastic case, the matrix element for transition to a state A_n is

$$
-i A_{A_0 \to A_n}^{q\bar{q}} = \sigma_p e^{-B_p \cdot \Delta^2/2} \sum_{i=1}^{A} \int d^2 \vec{b}_1 \cdots d^2 \vec{b}_A
$$
$$
\times \Psi_{A_n}^*(\vec{b}_1 \cdots \vec{b}_A) \Psi_{A_0}(\vec{b}_1 \cdots \vec{b}_A) \cdot e^{-i\vec{b}_i \cdot \vec{\Delta}}. \quad (19)
$$

The quasielastic dipole cross section,

$$
\sum_n \frac{d\sigma_{A_0 \to A_n}^{q\bar{q}}}{dt}
$$
$$
= \frac{1}{16\pi} \sum_n \left| A_{A_0 \to A_n}^{q\bar{q}} \right|^2
$$
$$
= \frac{\sigma_p^2}{16\pi} e^{-B_p \Delta^2} \sum_i^A \sum_j^A \int d^2 \vec{b}_1 \cdots d^2 \vec{b}_A d^2 \vec{b}'_1 \cdots d^2 \vec{b}'_A
$$
$$
\times \Psi_{A_0}^*(\vec{b}'_1 \cdots \vec{b}'_A) \cdot \sum_n \Psi_{A_n}(\vec{b}'_1 \cdots \vec{b}'_A) \Psi_{A_n}^*(\vec{b}_1 \cdots \vec{b}_A)
$$
$$
\times \Psi_{A_0}(\vec{b}_1 \cdots \vec{b}_A) \cdot e^{-i(\vec{b}_i - \vec{b}'_j) \cdot \vec{\Delta}},
$$

can be evaluated using the completeness relation,

$$
\sum_n \Psi_{A_n}(\vec{b}'_1 \cdots \vec{b}'_A) \Psi_{A_n}^*(\vec{b}_1 \cdots \vec{b}_A)
$$
$$
= \delta(\vec{b}_1 - \vec{b}'_1) \cdots \delta(\vec{b}_A - \vec{b}'_A), \quad (20)
$$

giving

$$
\sum_n \frac{d\sigma_{A_0 \to A_n}^{q\bar{q}}}{dt}
$$
$$
= \frac{\sigma_p^2}{16\pi} e^{-B_p \Delta^2} \sum_i^A \sum_j^A \int d^2 \vec{b}_1 \cdots d^2 \vec{b}_A
$$
$$
\times \Psi_{A_0}^*(\vec{b}_1 \cdots \vec{b}_A) \cdot \Psi_{A_0}(\vec{b}_1 \cdots \vec{b}_A) \cdot e^{-i(\vec{b}_i - \vec{b}_j) \cdot \vec{\Delta}}. \quad (21)
$$

_____

[9]This is like the Frauenhofer diffraction on a circular aperture.

Defining the two-nucleon distribution as

$$
\int d^2 \vec{b}_3 \cdots d^2 \vec{b}_A d^2 \Psi_{A_0}^*(\vec{b}_1 \cdots \vec{b}_A) \Psi_{A_0}(\vec{b}_1 \cdots \vec{b}_A)
$$
$$
= T_A^{(2)}(\vec{b}_1, \vec{b}_2), \quad (22)
$$

with normalization $\int d^2 b_1 d^2 b_2 T_A^{(2)}(\vec{b}_1, \vec{b}_2) = 1$, we obtain

$$
\sum_n \frac{d\sigma_{A_0 \to A_n}^{q\bar{q}}}{dt} = \frac{\sigma_p^2}{16\pi} e^{-B_p \Delta^2} \left[A + A(A-1) \right.
$$
$$
\left. \times \int d^2 \vec{b}_1 d^2 \vec{b}_2 T_A^{(2)}(\vec{b}_1, \vec{b}_2) \cdot e^{-i(\vec{b}_1 - \vec{b}_2) \cdot \vec{\Delta}} \right]. \quad (23)
$$

The first term in the square brackets, proportional to A, emerges from the summation of terms with $i = j$ in Eq. (21). The second term, proportional to $A(A-1)$, is obtained using the antisymmetry property of the wave function and the assumption that the difference between protons and neutrons can be neglected, $T_A^{(2)}(b_1, b_2) = T_A^{(2)}(b_i, b_j)$ for $i \neq j$.

The incoherent dipole cross section is obtained by subtracting the ground-state contribution from the sum of Eq. (23),

$$
\sum_{n \neq 0} \frac{d\sigma_{A_0 \to A_n}^{q\bar{q}}}{dt} = \frac{\sigma_p^2}{16\pi} e^{-B_p \Delta^2} \int d^2 \vec{b}_1 d^2 \vec{b}_2 \big\{ A \big(T_A(b_1) T_A(b_2)
$$
$$
- T_A^{(2)}(\vec{b}_1, \vec{b}_2) e^{-i(\vec{b}_1 - \vec{b}_2) \cdot \vec{\Delta}} \big) + A^2 \big(T_A^{(2)}(\vec{b}_1, \vec{b}_2)
$$
$$
- T_A(b_1) T_A(b_2) \big) e^{-i(\vec{b}_1 - \vec{b}_2) \cdot \vec{\Delta}} \big\}. \quad (24)
$$

When the momentum transfer $\Delta \to 0$ the incoherent dipole cross section, Eq. (24), goes to zero, reflecting the fact that, without a transfer of transverse momentum to the nucleus, excited states cannot be produced. At larger values of the momentum transfer, $|\vec{\Delta}| > 200$ MeV, the contribution of the second term in the curly brace in Eq. (24), $\int d^2 \vec{b}_1 d^2 \vec{b}_2 A (T_A^{(2)}(\vec{b}_1, \vec{b}_2) e^{-i(\vec{b}_1 - \vec{b}_2) \cdot \vec{\Delta}})$, starts to be relatively smaller than that of the first term because the oscillatory factor suppresses the contributions with $|\vec{b}_1 - \vec{b}_2| > 1$ fm. The contribution of the second term then grows as $A^{1/3}$ and can be neglected for larger nuclei, compared to the contribution of the first term, which grows as A. Thus when $|\vec{\Delta}| > 200$ MeV,

$$
\sum_{n \neq 0} \frac{d\sigma_{A_0 \to A_n}^{q\bar{q}}}{dt} = \frac{A d\sigma_{p \to p}^{q\bar{q}}}{dt} + \frac{\sigma_p^2}{16\pi} e^{-B_p \Delta^2} A^2 \int d^2 \vec{b}_1 d^2 \vec{b}_2
$$
$$
\times \big(T_A^{(2)}(\vec{b}_1, \vec{b}_2) - T_A(b_1) T_A(b_2) \big) e^{-i(\vec{b}_1 - \vec{b}_2) \cdot \vec{\Delta}}, \quad (25)
$$

and the deviation from the elastic nucleon cross section result is attributable to two-body correlations only.

Experimentally we expect to be able to distinguish cases where the nucleus remains intact and cases where the nucleus breaks up. In the nuclear breakup process, there are about $0.3\sqrt{A}$ free neutrons and $0.2\sqrt{A}$ protons in the final state [47], as well as other fragments. These particles and fragments have high momenta and different charge-to-mass ratios than the nuclear beam and should, therefore, be measurable in specialized detectors. However, we do not have a one-to-one correspondence between an intact nucleus and a coherent
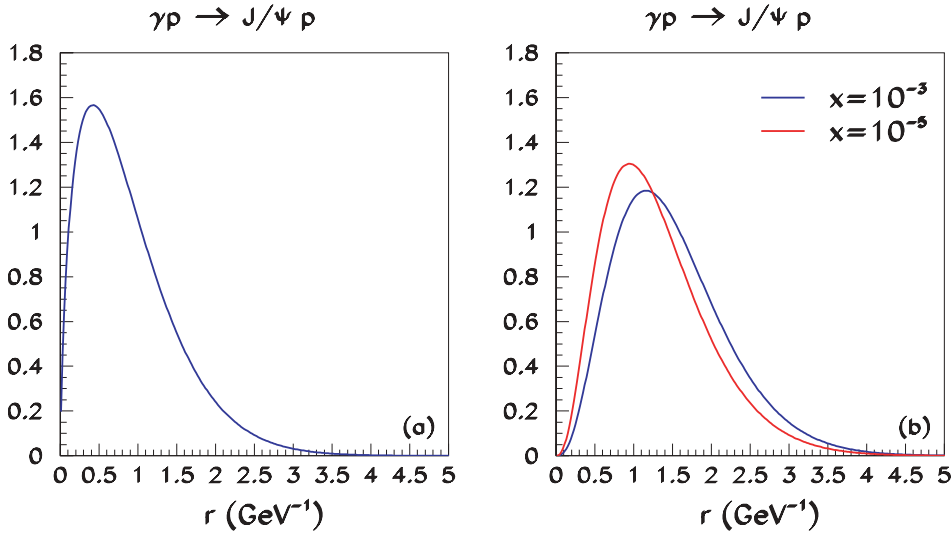
FIG. 9. (Color online) Distribution of J/ψ dipole sizes: (a) as given by the $\gamma J/\psi$ overlap function; (b) as given by the photoproduction amplitude.

scattering process, as incoherent processes can lead to an intact nucleus in an excited state. It remains to be determined how well excited states of the nucleus can be identified, measured, and possibly statistically subtracted to extract the fully separated coherent and incoherent processes.

C. Saturation

One of the main results of HERA is the observation that the gluon density increases quickly with decreasing x. This suggests that at some low x the dipole could undergo multiple interactions. The degree of saturation is characterized by the size of the dipole r_S, which, at a given x, starts to interact multiple times. The dipole size r_S is defined, by convention [18], via the relation[10]

$$\frac{d\sigma_{q\bar{q}}(x, r_S, b)}{d^2b} = 2(1 - \exp(-1/2)) \approx 0.8. \quad (26)$$

The saturation scale is then defined as $Q_S^2 = 2/r_S^2$ and is a function of x. A high value of the saturation scale means that the gluon density is so high that even small dipoles interact many times.

In various analyses of HERA data the saturation scale, in the proton center, was found to be $Q_S^2 \approx 0.5$ GeV^2 at $x \approx 10^{-3}$, that is, in the EIC range. In the LHeC range, which extends to $x \approx 10^{-5}$, the saturation scale could reach $Q_S^2 \approx 2$ GeV^2 [18]. The saturation scale determined in the inclusive $\gamma^* p$ reaction should be compared to the scale of J/ψ photoproduction given by the effective size of the meson in this reaction. This size is determined by the overlap of the photon and J/ψ wave functions and by the dynamical effects. Figure 9(a) shows the distribution of the dipole sizes selected by the overlap of the photon and J/ψ wave functions defined as $r \int dz \Psi_{J/\psi}^* \Psi$. The median value of this distribution is $r_{med}^o = 0.7$ GeV^{-1}, that is, about 0.15 fm. The contribution of very small dipoles, in

the γp reaction, is suppressed by the dynamic of the reaction, because the dipole cross section is proportional to r^2 at small r; see Eq. (9). The distribution of the dipole sizes selected by the amplitude, Eq. (7), is shown in Fig. 9(b). The median value of this distribution, r_{med}^a, was found[11] to be between 1.2 and 1.4 GeV^{-1}, depending somewhat on x. Thus, the effective scale characteristic for J/ψ photoproduction is $Q_{eff}^2 = 2/(r_{med}^a)^2 \approx$ 1–1.5 GeV^2, depending on x. The saturation scale at EIC is sizably smaller then Q_{eff}^2, so saturation effects are not expected to be large. However, the measurement on nuclei could enhance the saturation scale substantially, as discussed in Ref. [21]. Therefore, the high precision that can be achieved in the measurement of J/ψ exclusive photoproduction makes this process interesting as an alternative test bed of saturation effects at EIC. At LHeC saturation effects should be clearly visible in the scattering on the proton and presumably very strong in nuclear reactions.

In Ref. [9] it was proposed to investigate the effects of saturation in a systematic way by extracting from data $S^2(b)$, the square of the S matrix. The S matrix is directly connected to the dipole cross section by $d\sigma_{qq}/d^2b = 2[1 - \Re S(b)]$ as shown in Eq. (5). The S matrix can also be used to define the saturation condition because its square has a meaning for the survival probability, that is, the probability of no interaction. The equivalent definition to Eq. (26) then reads $S^2 = e^{-1} \approx$ 0.37. Figure 10 shows the survival probability for dipoles of different sizes scattering on the proton, at $b = 0$, where the gluon density reaches its maximum [17].

To reconstruct the S matrix at $b = 0$ for protons it is necessary to measure the t distribution up to about $|t| \approx$ 2 GeV^2.[12] At HERA this measurement could not be performed because the measurement of the t distribution had large systematic errors for $|t| > 1$ GeV^2 and a low statistical significance. The systematic uncertainties that plagued HERA

---

[10]From the unitarity limit the highest value of a dipole cross section is $d\sigma/d^2b = 2$; see Eq. (11).

[11]The evaluation was performed in the b-Sat model with the "boosted Gaussian" wave function, at $t = 0$.

[12]In the case of nuclei the measurement will require a much smaller t range than in the proton case.
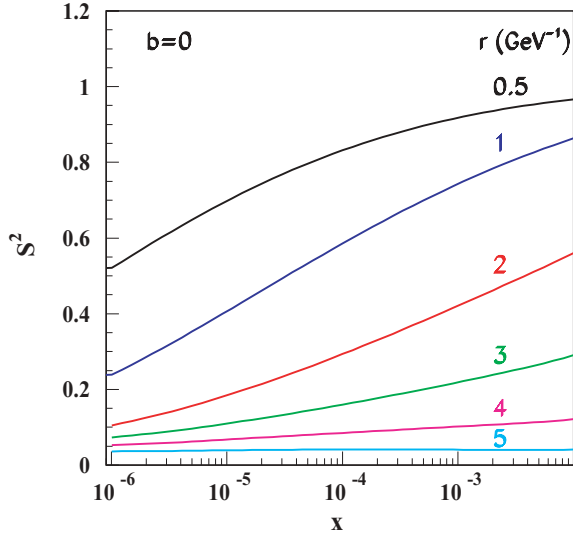
FIG. 10. (Color online) Survival probability S^2 as a function of x for various dipole sizes.

experiments can be avoided in the specially designed experiment discussed here. In addition, it should be possible to increase the collected number of events by about two orders of magnitude in comparison to HERA, which should allow us to reach the $|t| = 2$ GeV^2 region in the proton measurement.

IV. PRODUCTION CROSS SECTION

In this section, we review the production cross section for the photoproduction of J/ψ and discuss the kinematic range where high-precision measurements should be possible. The $ep \to epJ/\psi$ cross section can be written as

$$
\frac{d^2\sigma}{dW^2 dQ^2}
= \frac{\alpha}{2\pi} \frac{1}{s Q^2} \left[\left(\frac{1 + (1-y)^2}{y} - \frac{2(1-y)}{y} \frac{Q^2_{\min}}{Q^2} \right) \right.
$$
$$
\left. \cdot \sigma_T^{\gamma p}(W^2, Q^2) + \frac{2(1-y)}{y} \cdot \sigma_L^{\gamma p}](W^2, Q^2) \right],
$$

where

$$
Q^2_{\min} = \frac{m_e^2 y^2}{1 - y}
$$

and y is the inelasticity. We are interested in very small Q^2, for example, $Q^2 < 10^{-2}$ GeV^2, and we can assume that, in this range, the photoproduction cross section is independent of Q^2. We also assume that the longitudinal cross section is negligible, as we are dealing with almost-real photons. Then integration gives

$$
\frac{d\sigma}{dW^2} = \frac{\alpha}{2\pi} \frac{1}{s} \left[\frac{1 + (1-y)^2}{y} \ln \frac{Q^2_{\max}}{Q^2_{\min}} - \frac{2(1-y)}{y} \right.
$$
$$
\left. \times \left(1 - \frac{Q^2_{\min}}{Q^2_{\max}} \right) \right] \cdot \sigma^{\gamma p}(W^2) .
$$

From the ZEUS data [33], we have

$$
\sigma^{\gamma p \to J/\psi p}(W^2) \approx 75 \text{ nb} \left(\frac{W^2}{8100} \right)^{0.35} .
$$

Writing this in terms of y, we have

$$
\sigma^{\gamma p \to J/\psi p} = 75 \text{ nb} \left(\frac{s}{8100} \right)^{0.35} y^{0.35},
$$

where W is in GeV and s is in GeV^2. This form is valid at the large W measured at HERA. An extrapolation to lower values of W is in agreement with measurements performed by E401 [50], so we assume this form for all W.

We consider two different values of $Q^2_{\max}$. In one case, we assume that we do not measure the scattered electron precisely, and we can only limit the Q^2. For this case, we take $Q^2_{\max} = 10^{-4}$ GeV^2 so that the maximum p_T from the electron is 10 MeV. In the second case, we assume that we do measure the scattered electron well, so we can afford to go to higher Q^2, and we take $Q^2_{\max} = 10^{-2}$ GeV^2. In the Q^2 range considered here, the scattered electron energy is given by $E' = (1 - y)E_e$.

High-precision measurements of the J/ψ decay products are assumed to be made in a central detector, such as a thin-walled time projection chamber, located in a strong solenoidal magnetic field. The detector parameters are discussed in the next section. To measure the J/ψ decay products with good acceptance in the central detector, we require that the J/ψ has limited boost. For simplicity, we take $Q^2 = t = 0$ to see the limits on y [49]. Conservation of energy gives

$$
E_e + E_p = (1 - x)E_p + E'_e + E_V,
$$

where E_e, E_p are the incoming beam energies, and E'_e, E_V are the scattered electron and vector-meson energies. This can be rewritten as

$$
x = \frac{E_V - yE_e}{E_p}.
$$

We also have the requirement,

$$
M_V^2 = (xp + q)^2 \approx 2xp \cdot q \approx sxy,
$$

or

$$
x = \frac{M_V^2}{sy}.
$$

Putting these expressions together gives

$$
E_V \approx y \cdot E_e + \frac{M_V^2}{4yE_e},
$$

where M_V is the mass of the J/ψ. This leads to the following constraints:

$$
y_{\max} = \min \left[1, \frac{E_V + P_V}{2E_e} \right],
$$
$$
y_{\min} = \max \left[0, \frac{E_V - P_V}{2E_e} \right],
$$

or, in terms of W^2,

$$
W^2_{\max} = sy_{\max},
$$
$$
W^2_{\min} = sy_{\min}.
$$

We now integrate the differential cross section given above in this W^2 range, with the result

$$\sigma(\text{visible}) = A\frac{\alpha}{2\pi}\left(\frac{s}{8100}\right)^b\left[\frac{2(c-1)}{b}y^b + \frac{2(1-c)}{1+b}y^{1+b}\right.$$
$$\left.+ \frac{c}{2+b}y^{2+b}\right]_{y_{\min}}^{y_{\max}},$$

where we have

$$A = 75.\ \text{nb},$$
$$b = 0.35,$$
$$c = \ln\frac{Q^2_{\max}}{Q^2_{\min}}.$$

To see the effect of the centrality requirement, we require that the momentum of the J/ψ be less than 4 GeV, so that the decay particles are not too boosted. We performed a scan over electron beam energy, keeping the proton beam energy fixed at $E_p = 100$ GeV. The accepted y ranges are shown in Fig. 11. The results for the visible cross section (not including the branching ratio) are given in Fig. 12. Adding the branching ratio of about 6% implies that 10 fb^{-1} would give 10^6 well-reconstructed $J/\psi \rightarrow \mu^+\mu^-$ events in the central part of the detector.

FIG. 12. Visible J/ψ cross section as a function of the electron beam energy at $E_p = 100$ GeV.

V. EXPERIMENTAL CONSIDERATIONS

In the following, we consider the requirements for the beam momentum spread and the detector requirements for the scattered electron, the measurement of the J/ψ, and the measurement of the scattered nucleus or proton. As discussed in Sec. III B and Sec. II C, the proton or nuclear shapes are measured by the deflection of the J/ψ from its original direction. The t measurement will rely on an accurate determination of the transverse momentum given to the J/ψ, as

$$t = (p_i - p_f)^2 \approx -((\Delta p_x)^2 + (\Delta p_y)^2),$$

where p_i, p_f are the momenta of the incoming photon and outgoing J/ψ, and Δp_x, Δp_y are the changes in the transverse momentum components during the scattering process. As is clear from these expressions, we require knowledge of (a) the outgoing J/ψ momentum and (b) the incoming and outgoing electron momenta, as

$$\vec{p}_{e,i} - \vec{p}_{e,f} - \vec{p}_{J/\psi} = \vec{p}_i - \vec{p}_f.$$

Usually, t is viewed as a change in the momentum of the incoming and the outgoing ions or protons, $t = -(\vec{p}_{I,i} - \vec{p}_{I,f})^2$. Measurement of the ion momenta is technically very difficult. Here, it is not necessary because $\vec{p}_{I,i} - \vec{p}_{I,f} = \vec{p}_{e,f} + \vec{p}_{J/\psi} - \vec{p}_{e,i}$. We, therefore, do not foresee a precise measurement of the ion p_T.

Measuring the outgoing J/ψ and electron (or guaranteeing that the outgoing electron has a very small transverse momentum) then allows measurement of t. Nevertheless, the forward scattering region for the ions will require substantial instrumentation (a) to guarantee that we have an elastic scattering event and (b) to measure the correlation between the variable t and the transverse momenta of debris from the nuclear dissociation in inelastic events.

We discuss the separate parts of the detector system according to their function. Because we are dealing with photoproduction, the large majority of the events are
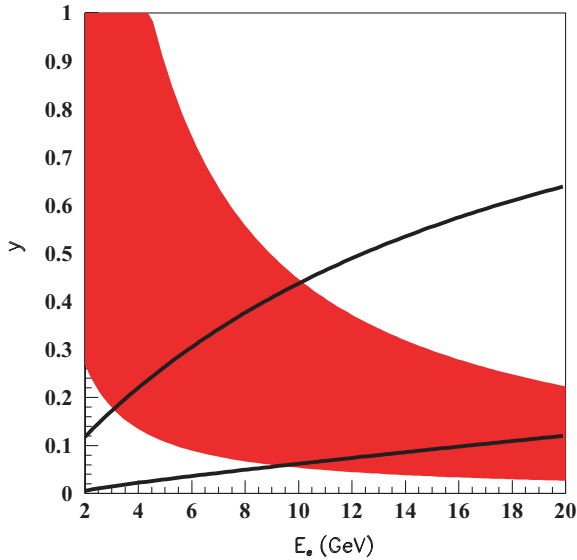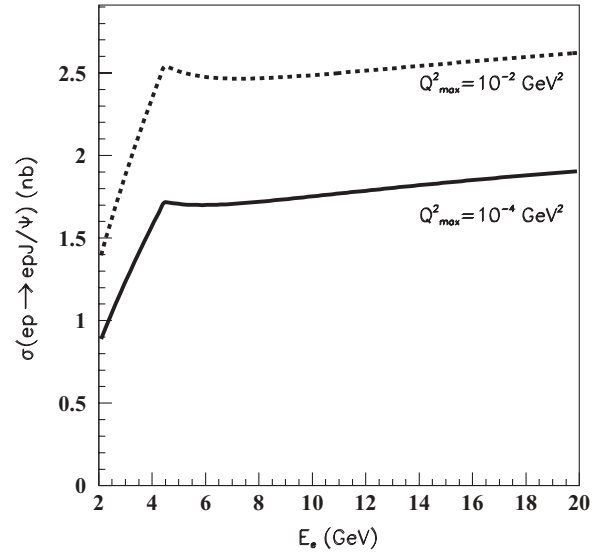

FIG. 11. (Color online) The y range with good acceptance for reconstructing J/ψ decays in the central region is plotted as a function of the electron beam energy [shaded (red) area] at $E_p = 100$ GeV. The two curves indicate the minimum y values for detecting the beam electron scattered at $0°$ assuming (upper curve) that a 1-Tm dipole is placed near the interaction point (IP) and that the scattered electron should be at least 5 cm from the beam 5 m downstream of the dipole and assuming (lower curve) that a 5-Tm dipole is placed near the IP and that the scattered electron should be at least 5 cm from the beam 10 m downstream of the dipole.

concentrated close to $Q^2 = 0$ GeV^2. The scattered electron will therefore have a median transverse momentum of only a few megaelectronvolts. As discussed below, it should be possible to measure this scattered electron over the bulk of the kinematic range of interesst. Even in cases where the electron is not detected, it will typically only carry a very small transverse momentum. The measurement of the t distribution will therefore rely almost exclusively on a precise measurement of the J/ψ decay products.

A. Scattered electron

The scattered electron will be at a very small angle to the direction of the electron beam but can be pulled out of the beam if it has lost enough energy. There will be a minimum value of y where it is possible to see the scattered electron even if the electron is scattered at $0°$. For this purpose, we imagine that there will be a large-aperture dipole magnet placed near the beam interaction point, which will bend the electrons (and can also act as a separator of the ion and electron beams). The transverse separation between a beam electron and a forward scattered electron can be written as

$$\Delta = D \left[\sin\theta_y \frac{\cos\theta_0}{\cos\theta_y} - \sin\theta_0 \right],$$

where

$$\sin\theta = \frac{0.3 \cdot B \cdot L}{p},$$

with the dipole field strength B measured in T, the length of the magnet L in m, and the momentum of the electron p in GeV/c. θ_0 is used to denote the scattering angle of the beam electrons after passage through the dipole, and θ_y is the scattering angle for momentum $p = (1 - y)E_e$. The distance D is measured from the center of the dipole. If detectors are placed within a few centimeters from the electron beam a few meters downstream of the dipole magnet, then scattered electrons at a not-too-low y can be measured. The minimum value of y required for acceptance of such a system depends on the strength of the dipole field, the distance of approach to the beamline, and the drift distance D. Figure 11 indicates the minimum y values as a function of the electron beam energy for two representative sets of parameter values. We conclude that measuring the scattered electron will be feasible over the bulk of the y range of interest that provided the interaction region allows for such a dipole magnet and detector arrangement.

B. J/ψ reconstruction

We focus on measurement of the J/ψ via the decay into muons, $J/\psi \to \mu^+\mu^-$. We assume that no particle identification will be necessary, as it will be easy to identify the J/ψ via the invariant mass of the reconstructed state. A continuous background from the Bethe-Heitler process $eA \to eA\mu^+\mu^-$ will have to be handled in the analysis of the data. The expected resolution of the drift chamber can be estimated from the measurement precision term,

$$(\sigma_{p_t}/p_t)_{\text{meas}} = \frac{p_t \, \sigma_{r\phi}}{0.3L^2 B} \sqrt{\frac{720}{N+4}},$$

and the multiple scattering contribution,

$$(\sigma_{p_t}/p_t)_{\text{MS}} = \frac{0.05}{LB\beta} \sqrt{1.43 \frac{L}{X_0}} [1 + 0.038 \log(L/X_0)],$$

as

$$\sigma_{p_t}/p_t = (\sigma_{p_t}/p_t)_{\text{meas}} \oplus (\sigma_{p_t}/p_t)_{\text{MS}}.$$

Here B is the magnetic field in tesla, L is the lever arm in meters, $\sigma_{r\phi}$ is the spatial resolution in meters for a single point, X_0 is the radiation length in meters, N is the number of points, and β is the velocity of the particle.

In the J/ψ photoproduction process at small t the transverse momenta of the decay muons range from very small values up to a maximum of about 2 GeV/c. In this momentum range, multiple scattering is a critical issue for momentum resolution. We therefore envision a time projection chamber (TPC)-type detector with a thin inner wall as the central tracking detector. Assuming the following parameters,

(i) outer radius $R = 2$ m,
(ii) solenoidal field $B = 3.5$ T,
(iii) gas density $X_0 = 450$ m,
(iv) point resolution $\sigma = 100$ μm, and
(v) measurement $N = 200$ points,

yields a track momentum resolution [48],

$$\sigma_{p_t}/p_t = 0.005 \cdot p_t \oplus 0.045/\beta\%,$$

which will give a p_t resolution for the J/ψ of typically $\leqslant 1$ MeV.

The muons would not escape such a detector in the radial direction. An electromagnetic calorimeter placed outside the TPC could be used to reject or measure radiated photons from the interaction vertex and from passage of the muons through the detector. The detector design could naturally be extended to include hadronic calorimetry, particularly in the ion direction, resulting in a general-purpose detector capable of high-precision measurements for all types of exclusive processes as well as inclusive cross-section measurements.

C. Ion forward direction

The main requirement for the instrumentation in the forward direction of the ion beam is that dissociative and inelastic events be rejected with ∼100% efficiency. We envisage again a dipole magnet that can be used to separate neutral particles as well as nuclear fragments from the main beam. This dipole could also serve as a beam separator to guide the electrons and ions to their individual beampipes. Ion dissociation will produce different types of fragments, including neutrons and charged ions with charge/mass ratios different from that of the beam ions. Neutrons can be recorded in a calorimeter at $0°$ to the beamline at the interaction point and located many meters downstream of the interaction point. Fragments with different charge/mass ratios will have different deflection angles in the dipole than the main beam and can, therefore, be measured with tracking detectors placed close to the beamline. In inelastic scattering events, particles with opposite charge to the beam ions can be produced, and these interactions can be

vetoed using tracking detectors or calorimeters placed behind the dipole. We therefore expect that for large nuclei, rejecting nonelastic events will be rather straightforward, as typically several neutrons and charged particles will be produced.

D. Beam requirements

The experiment discussed requires substantial instrumentation extending to many meters on either side of the interaction point. It will be critical to avoid "dead zones," where scattered particles could escape detection. This will place severe restrictions on the accelerator design and will naturally lead to limitations in luminosity. The detector design foresees a central region with a strong solenoidal field and dipole magnets on either side of the interaction point (perhaps ± 2 m away). The design of these magnets will necessarily have to be done in conjunction with the accelerator group. Issues such as synchroton radiation loads will need to be evaluated. In addition, it is critical that the electron beam transverse momentum be limited to a few megaelectronvolts, as this quantity cannot be measured but enters into the calculations of t.

VI. SUMMARY AND DISCUSSION

We have discussed here the physics potential of t measurements. At HERA, the measurement of t distributions allows determination of the two-gluon proton radius. This radius is substantially smaller than the proton radius determined in the electromagnetic interactions, $r_{2g} < r_p$.

To exemplify the potential of such measurements in future electron-ion colliders, we have considered two simple examples of coherent and incoherent J/ψ dipole scattering on nuclei. In the coherent case the nucleus remains intact, while in the incoherent case the nucleus goes into any excited state or it disintegrates into nucleonic fragments or nucleons without production of additional hadrons.

In the coherent case we have computed the predictions of the dipole model assuming that nucleons are distributed within the nucleus according to the Woods-Saxon distribution (Fig. 8), which is mainly determined by scattering on the electric charges. It is very possible that, as in the proton case, the nuclear radius and skin parameters can be quite different when measured by elastic J/ψ scattering. The shape of the expected cross section and the differences between different predictions indicate that a measurement resolution of about 10 MeV for the p_T of J/ψ should be sufficient. This number emerges from the requirement that the first diffractive minimum should be properly resolved.

Incoherent J/ψ scattering is equally interesting, as the very good p_T resolution combined with the full acceptance detector discussed here should allow a systematic study of the two-body correlations. Measurement of the long-range nuclear correlations could require a measurement resolution of O(1) MeV in p_T of the J/ψ decay products.

The t distribution of the nuclear breakup process will be measured in correlation with the number and momenta of the breakup protons and neutrons. This should allow study of the dissociation process as a function of the transverse momentum transferred to the nucleus.

Although we have concentrated here on the measurement of J/ψ decays, it should be clear that the detector that is optimal for measurements of J/ψ elastic scattering will also be optimal for measurements of other interactions, like light vector-meson production and inclusive diffractive or inclusive total cross sections. The quality of the inclusive measurements will also profit from the large acceptance detector discussed here because the coverage of the almost-entire rapidity range for charge and neutral particles will reduce the systematic uncertainties in the F_2 and F_2^D measurements.

The nuclear effects will also be seen through the measurement of the absolute value of cross sections. The dipole model predicts these values precisely provided that the scattering takes place on nucleons within the nucleus that have the same properties as free protons. Any deviation from the expected value carries information about nuclear effects. For example, the total dipole proton cross section σ_p can be different for a nucleon in a nucleus than for a proton because a nucleon within a nucleus can have a different size from that of a free proton or neutron. This would change considerably the value of the nuclear dipole cross section and therefore also the values of the observed diffractive cross sections. By the same argument the measurement of F_2 on nuclei is also determined by the nuclear properties and will lead to very interesting saturation effects as discussed in Refs. [17] and [21]. Saturation is dependent on the size of the scattering objects, therefore its measurement and the absolute value of the cross section could indicate on what objects the scattering takes place.

The measurement of the transverse shape and correlations combined with the measurements of the total cross sections and the shadowing effects should allow determination of the inner structure of gluonic fields that keep the nuclei together.

VII. CONCLUSION

We have shown that scattering of small dipoles can become an important source of information on the gluonic structure of nuclei. At high energies, the dipoles interact with nuclei by a well-understood QCD process in which two gluons, with large transverse momenta, are exchanged. The difference in the gluon momenta can be precisely determined by measuring the transverse momentum of the elastically scattered vector meson. The J/ψ photoproduction process is particularly well suited to perform this measurement because it has the largest cross section and the best measurement precision. The p_T of J/ψ can be measured with a high efficiency and a precision of O(1) MeV using presently available techniques. This allows determination of the t distributions with a precision of O(1) MeV^2, starting at $t \approx 0$. The upper range of the available t values depends on the process and can reach O(3) GeV^2 with the luminosity foreseen at EIC or LHeC. This allows investigation of large and/or small gluonic structures that keep the matter together. It is worth emphasizing that large structures are investigated by a highly virtual, well-understood interaction because a small p_T of the J/ψ meson is a result
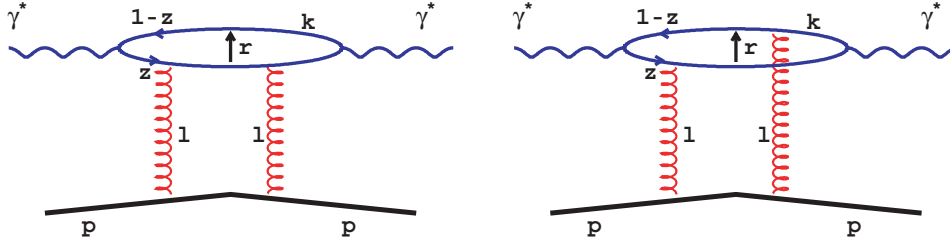
FIG. 13. (Color online) Elastic photon-proton scattering at $t = 0$.

of the difference in two large transverse gluon momenta. Therefore, dipole measurements will provide high-quality data of a basic nature, which could lead to solution of the long-standing puzzle: how strong interactions form matter.

ACKNOWLEDGMENTS

APPENDIX

A. Derivation of the dipole representation

We give here a derivation of the dipole representation for elastic $\gamma^* p \to \gamma^* p$ scattering to exemplify the main properties of the dipole picture. Dipoles incorporate naturally the interference effects between different quark-gluon couplings that are essential to obtain a proper description of DIS reactions at low x, namely, color transparency.[13] For the sake of illustration, let us consider the scattering of a longitudinally polarized virtual photon on a proton. Following the derivation given in Refs. [8,14,15], we write the total cross section in the k_T factorization form according to the Feynman diagrams shown in Fig. 1 as

$$\sigma_L = \frac{\alpha_{\mathrm{em}}}{\pi} \sum_f e_f^2 \int \frac{d^2\vec{l}}{l^4} \alpha_s f(x, l^2) \int d^2\vec{k}$$

$$\times \int dz \, 4Q^2 z^2 (1-z)^2 \left(\frac{1}{D(\vec{k})} - \frac{1}{D(\vec{k}+\vec{l})} \right), \quad (A1)$$

where $D(\vec{k}) = \vec{k}^2 + \bar{Q}^2$ and $\bar{Q}^2 = z(1-z)Q^2 + m_f^2$. Here m_f denotes the flavor-dependent quark mass and $f(x, l^2)$ denotes the unintegrated gluon density. In the $\gamma^* p$ collinear frame $\vec{k}$ and $\vec{l}$ are the two-dimensional transverse momentum vectors of the quark and the exchanged gluon and z and $(1-z)$ are the fractions of the light-cone momentum of the photon carried by the quarks.

---

[13]Although we limit ourselves in this paper to ep and eA scattering, let us note that the dipole concept, because of its importance in understanding the QCD evolution [23] and its success at HERA, is now extensively investigated also in the context of pp scattering at the LHC [24].

In the elastic forward scattering there are just two possibilities for gluons to couple to the quarks, shown in the two diagrams in Fig. 13. Both diagrams should be taken into account because only then does the important property of color transparency emerge from the cancellation between the two propagators in Eq. (A1). In the limit $k \gg l$ the cancellation leads to $\sigma_L \approx 0$, reflecting the intuitively clear fact that a gluon cannot see a quark pair when its wavelength is much larger than the distance between the quarks. In this case, the quark pair will appear as neutral to the gluon.

Color transparency emerges more naturally when the transverse quark momentum $\vec{k}$ is replaced by its Fourier conjugate $\vec{r}$, the transverse separation between the two quarks. We then have

$$\int \frac{d^2\vec{k}}{2\pi} \exp(i\vec{k}\vec{r}) \frac{1}{D(\vec{k})} = K_0(r \cdot \bar{Q})$$

and

$$\left(\frac{1}{D(\vec{k})} - \frac{1}{D(\vec{k}+\vec{l})} \right)$$

$$= \int \frac{d^2\vec{r}}{2\pi} \exp(-i\vec{k}\vec{r})(1 - \exp(-i\vec{l}\vec{r})) K_0(r \cdot \bar{Q}),$$

with K_0 being the Bessel-McDonald function.

The change of variables from $\vec{k}$ to $\vec{r}$ leads to the dipole representation,

$$\sigma_L = \mathrm{Im} A^{\gamma^* p}(x, Q, \vec{\Delta} = 0) = \int d^2\vec{r} \int dz \sum_f \Psi_L^*(r, z, Q^2)$$

$$\times \sigma_{qq}(x, r) \Psi_L(r, z, Q^2), \quad (A2)$$

in which the wave function Ψ_L describes the probability amplitude to find a $q\bar{q}$ pair within a virtual incoming or outgoing photon:

$$\Psi_L^2 = \frac{3\alpha_{\mathrm{em}}}{2\pi^2} e_f^2 4Q^2 z^2 (1-z)^2 K_0^2(r \cdot \bar{Q}).$$

The dipole cross section σ_{qq} describes the interaction of the $q\bar{q}$ pair with the proton mediated by the two-gluon exchange.

$$\sigma_{qq} = \frac{2\pi}{3} \int \frac{d^2\vec{l}}{l^4} \alpha_s f(x, l^2)(1 - e^{-i\vec{l}\vec{r}})(1 - e^{i\vec{l}\vec{r}})$$

$$= \frac{4\pi^2}{3} \int \frac{dl^2}{l^4} \alpha_s f(x, l^2)(1 - J_0(lr)).$$

By introducing the relation between the integrated and the unintegrated gluon density,

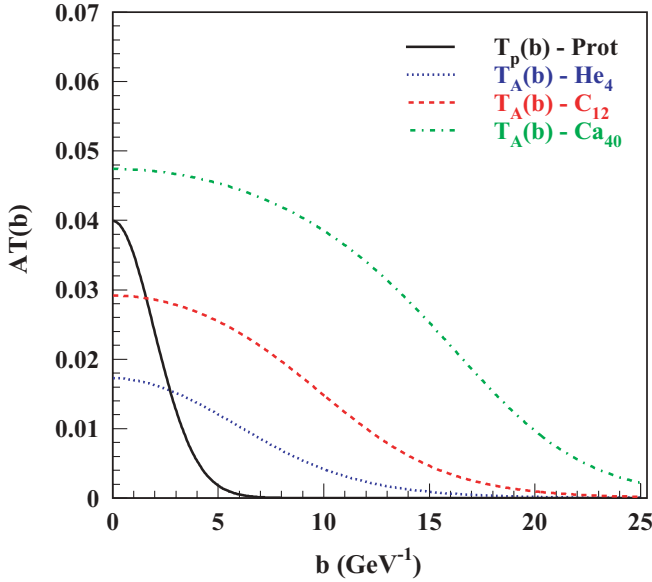$$xg(x, Q^2) = \int_0^{Q^2} dl^2 f(x, l^2)/l^2, \quad (A3)$$

FIG. 14. (Color online) Transverse density, $A\,T_{\mathrm{WS}}(b)$, for several light nuclei compared to the proton transverse profile, $T_p(b)$.

and assuming that α_s depends on the dipole size only, the dipole cross section can be further simplified by approximating $(1 - J_0(lr)) \approx (lr)^2/4$, which is valid for $l^2 < 1/r^2$:

$$\sigma_{qq} = \frac{\pi^2}{3} \alpha_s(1/r^2) r^2 x g(x, 1/r^2). \qquad \text{(A4)}$$

Here $xg(x, \mu^2)$ is the gluon distribution that evolves in $\mu^2 = 1/r^2$ according to the DGLAP evolution equation.

In this representation color transparency becomes a property of the dipole cross section; for small dipoles $r \to 0$ and, also, $\sigma_{qq} \to 0$, as is intuitively clear. The last form of the dipole cross section was first derived in Ref. [16] in an alternative way.

B. Woods-Saxon distribution

The distribution of nucleons in the nucleus $\rho_A(r)$ is usually parametrized according to the Woods-Saxon distribution [42],

$$\rho_{\mathrm{WS}}(r) = \frac{N}{\exp\left(\frac{(r - R_A)}{\delta}\right) + 1}, \qquad \text{(A5)}$$

where $\delta = 0.54$ fm, $R_A = (1.12\text{ fm})A^{1/3} - (0.86\text{ fm})A^{-1/3}$, and N is adjusted to normalize the distribution to

$$\int d^3\vec{r}\, \rho_{\mathrm{WS}}(r) = 1. \qquad \text{(A6)}$$

The transverse distribution is defined as

$$T_{\mathrm{WS}}(b) = \int_{-\infty}^{+\infty} dz \rho_{\mathrm{WS}}(\sqrt{b^2 + z^2}). \qquad \text{(A7)}$$

Figure 14 compares the proton shape $T_p(b)$ with the transverse density $T_{\mathrm{WS}}(b)$ for several light nuclei.

[1] N. Ishii, S. Aoki, and T. Hatsuda, Phys. Rev. Lett. **99**, 022001 (2007).

[2] F. Wilczek, Nature **445**, 156 (2007).

[3] S. R. Beane, presented at the 26th International Symposium on Lattice Field Theory (Lattice 2008), Williamsburg, VA, 14–20 July 2008; arXiv:0812.1236 [hep-lat].

[4] J. Nemchik, N. N. Nikolaev, E. Predazzi, and B. G. Zakharov, Z. Phys. C **75**, 71 (1997).

[5] E. Gotsman, E. Levin, and U. Maor, Nucl. Phys. **B464**, 251 (1996).

[6] H. G. Dosch, T. Gousset, G. Kulzinger, and H. J. Pirner, Phys. Rev. D **55**, 2602 (1997).

[7] K. Golec-Biernat and M. Wüsthoff, Phys. Rev. D **59**, 014017 (1998); **60**, 114023 (1999).

[8] J. Bartels, K. Golec-Biernat, and H. Kowalski, Phys. Rev. D **66**, 014001 (2002).

[9] S. Munier, A. M. Staśto, and A. H. Mueller, Nucl. Phys. **B603**, 427 (2001).

[10] A. C. Caldwell and M. S. Soares, Nucl. Phys. **A696**, 125 (2001).

[11] J. R. Forshaw, R. Sandapen, and G. Shaw, Phys. Rev. D **69**, 094013 (2004).

[12] L. Frankfurt, M. Strikman, and C. Weiss, Annu. Rev. Nucl. Part. Sci. **55**, 403 (2005).

[13] H. Kowalski, T. Lappi, C. Marquet, and R. Venugopalan, Phys. Rev. C **78**, 045201 (2008).

[14] N. N. Nikolaev and B. G. Zakharov, Z. Phys. C **49**, 607 (1991); **53**, 331 (1992).

[15] K. Golec-Biernat, Habilitation thesis, Henryk Niewodniczanski Institute of Nuclear Physics, Report No. 1877/PH, 2001; www.ifj.edu.pl/publ/reports/2001/1877.pdf.

[16] L. Frankfurt, A. Radyushkin, and M. Strikman, Phys. Rev. D **55**, 98 (1997).

[17] H. Kowalski and D. Teaney, Phys. Rev. D **68**, 114005 (2003).

[18] H. Kowalski, L. Motyka, and G. Watt, Phys. Rev. D **74**, 074016 (2006).

[19] G. Watt and H. Kowalski, Phys. Rev. D **78**, 014016 (2008).

[20] E. Iancu, K. Itakura, and S. Munier, Phys. Lett. **B590**, 199 (2004).

[21] H. Kowalski, T. Lappi, and R. Venugopalan, Phys. Rev. Lett. **100**, 022303 (2008).

[22] H. Kowalski, T. Lappi, C. Marquet, and R. Venugopalan, arXiv:0805.4809.

[23] A. H. Mueller, Nucl. Phys. **B415**, 373 (1994); A. H. Mueller and B. Patel, *ibid.* **B425**, 471 (1994); A. H. Mueller, *ibid.* **B437**, 107 (1995).

[24] E. Avsar, G. Gustafson, and L. Lönnblad, J. High Energy Phys. 07 (2005) 062; 01 (2007) 012.

[25] A. Aktas *et al.* (H1 Collaboration), Eur. Phys. J. C **46**, 585 (2006).

[26] R. J. Glauber, Phys. Rev. **99**, 1515 (1955).

[27] A. H. Mueller, Nucl. Phys. **B335**, 115 (1990).

[28] M. Klasen and G. Kramer, Mod. Phys. Lett. A **23**, 1885 (2007).

[29] A. G. Shuvaev, K. J. Golec-Biernat, A. D. Martin, and M. G. Ryskin, Phys. Rev. D **60**, 014015 (1999); see also D. Müller, presented at DIS 09 Workshop, Madrid, 2009.

[30] J. Kwiecinski, A. D. Martin, and A. M. Stasto, Phys. Rev. D **56**, 3991 (1997).

[31] J. R. Forshaw, R. Sandapen, and G. Shaw, arXiv:hep-ph/0608161.

[32] A. Aktas *et al.* (H1 Collaboration), Eur. Phys. J. C **44**, 1 (2005); S. Chekanov *et al.* (ZEUS Collaboration), Phys. Lett. **B573**, 46 (2003); F. D. Aaron *et al.* (H1 Collaboration), *ibid.* **B659**, 796 (2008); I. Rubinsky (ZEUS Collaboration), presented at International Europhysics Conference on High Energy Physics (EPS-HEP2007), Manchester, England, 19–25 July 2007 [ZEUS-prel-07-016].

[33] S. Chekanov *et al.* (ZEUS Collaboration), Eur. Phys. J. C **24**, 345 (2002); Nucl. Phys. **B695**, 3 (2004).

[34] C. Adloff *et al.* (H1 Collaboration), Eur. Phys. J. C **13**, 371 (2000).

[35] S. Chekanov *et al.* (ZEUS Collaboration), Nucl. Phys. **B718**, 3 (2005).

[36] S. Chekanov *et al.* (ZEUS Collaboration), PMC Phys. A **1**, 6 (2007).

[37] ZEUS Collaboration, *XXII International Symposium on Lepton-Photon Interactions*, Uppsala, 2005, Session QCD/HS, Abstract 295 and Addendum.

[38] J. Bartels and H. Kowalski, Eur. Phys. J. C **19**, 693 (2001).

[39] M. Strikman and C. Weiss, Phys. Rev. D **69**, 054012 (2004).

[40] M. Diehl, presented at the Trento Workshop, 16 July 2008.

[41] U.-G. Meissner, Phys. Rep. **161**, 213 (1988).

[42] A. Bohr and B. R. Mottelson, *Nuclear Structure* (Benjamin, New York, 1969).

[43] J. Nemchik, N. N. Nikolaev, and B. G. Zakharov, Phys. Lett. **B341**, 228 (1994).

[44] J. Nemchik, N. N. Nikolaev, E. Predazzi, and B. G. Zakharov, Z. Phys. C **75**, 71 (1997).

[45] J. Bartels, K. Golec-Biernat, and K. Peters, Acta Phys. Pol. B **34**, 3051 (2003).

[46] A. Mueller (personal communication).

[47] J. Ranft and J. T. Routti, Part. Accel. **4**, 101 (1972).

[48] H. Hirano *et al.* (Belle Collaboration), NIM A **455**, 294 (2000).

[49] B. Mellado, Ph.D. thesis, Columbia University, Report DESY-Thesis-2002-002, 2002.

[50] M. Binkley *et al.* (E401 Collaboration), Phys. Rev. Lett. **48**, 73 (1982).